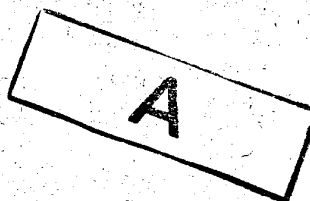
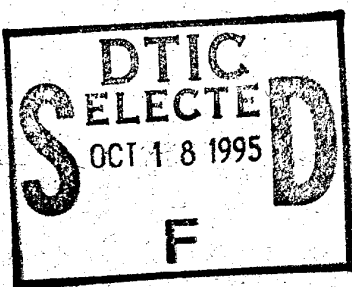


BR-311185①

UNLIMITED

48pp



DEFENCE RESEARCH AGENCY MALVERN

MEMORANDUM No. 4532

A THEORY FOR HYBRID SAR/ISAR RADAR IMAGING

Authors: R J A Tough & K D Ward

DISTRIBUTION STATEMENT A

Approved for public release
Distribution Unlimited

DEFENCE RESEARCH AGENCY,
MALVERN,
WORCS.

Processed / not processed by DIMS

..... signed date

NOT FOR DESTRUCTION

MEMORANDUM No. 4532

UNLIMITED

1995 10 13 040

MEMORANDUM 4532

Title: A THEORY FOR HYBRID SAR/ISAR RADAR IMAGING

Authors: R. J. A. Tough and K. D. Ward

Date: October 1991

SUMMARY

A unified treatment of the SAR and ISAR imaging processes is presented, in which each emerges as a special case of a more general hybrid SAR/ISAR process. Several such special cases are considered, demonstrating the simplicity and flexibility of our analysis whose results are also verified directly by computer simulation.

| | |
|---------------------|---------------------------|
| Accesion For | |
| NTIS | CRA&I |
| DTIC | TAB |
| Unannounced | |
| Justification | |
| By | |
| Distribution / | |
| Availability Codes | |
| Dist | Avail and / or Special |
| A-1 | |

© British Crown Copyright 1991/MOD
Published with the permission of the
Controller of Her Britannic Majesty's
Stationery Office

1995 1013 040

INTENTIONALLY BLANK

Introduction

Any ship on the sea surface is subject to rotational motions (yaw, pitch and roll) due to the sea's movements. Furthermore it is frequently convenient to survey maritime scenes from a moving radar platform. Both these motions will affect the imaging of a ship target and can be exploited, through suitable signal processing, to enhance the imagery obtained. Thus, if a stationary target is observed from a moving platform it is possible to synthesise coherently a large effective aperture and so to enhance azimuthal resolution (SAR). Conversely differential Doppler processing of the returns to a stationary platform from a rocking ship can provide more detailed across range information on the structure of the target through the technique of inverse synthetic aperture radar (ISAR). Target motions and, in particular, rotations will degrade SAR imagery; ISAR images are also adversely affected by radar platform motions. Unfortunately the standard descriptions of SAR and ISAR are couched in terms which make the analyses of these effects complicated and their physical basis and practical implications rather obscure. Consequently it is desirable to construct a theory of Hybrid SAR/ISAR imaging which treats target and platform motions on an equal footing, both to analyse the degradation of conventional SAR and ISAR images and to identify ways in which these hybrid images may be processed optimally. Such a theory, and some of its preliminary applications, will be described in this report.

In broad outline there are three concepts which underpin our analysis. These are the description of the imaging process in terms of Fourier transformation, the concise and correct representation of rotations and the analysis of image degradation in terms of the manner in which spatial Fourier components of the target are selected by rotational motions. The first of these ideas, which was introduced into the discussion of radar imaging by Walker^[1], allows us to unify the description of SAR and ISAR and so paves the way to a systematic analysis of the imagery obtained. The description of the rotational motions will require the introduction of a formalism which, while it is perhaps a little unfamiliar at first sight, provides us with a powerful tool for the analysis of the effects of target and platform motions in a general, simple and readily visualised manner. Finally, by bringing together these basic ideas it is possible to characterise the point spread or imaging function in terms of simple geometrical concepts which greatly facilitate the discussion of the imaging process. The relationship between our description of the SAR and ISAR processes and the standard analyses is discussed in an appendix. Similarly the details of the rotation formalism have been discussed elsewhere^[2] and will be quoted here, supported only by plausibility arguments rather than by a full analysis. Having set up our formalism we will analyse the SAR, ISAR and hybrid SAR/ISAR processes in some detail and make a preliminary comparison with computer simulation results, which provide a most satisfactory confirmation of our analysis.

Imaging and Fourier Transformation

In this section we will discuss the way in which the Fourier transform arises naturally in the description of the imaging process and can be used to characterise the images obtained in a simple fashion. This will lead us to a general 'master formula' which, when supplemented by our subsequent discussion of rotational motions, will allow us to analyse shifts, distortions and defocussing effects in a systematic fashion.

We consider a target whose position and orientation vary with time t and whose spatial extent over coordinates \underline{r}_o is specified by the scattering function $V(\underline{r}_o, t)$. The following reasonable assumptions can be made: That there is no shadowing or, more realistically, that shadowing is unchanged over angles of view sampled in the imaging process and that there are no non-linear or dispersive effects. For a monostatic radar platform, positioned at $\underline{r}(t)$ (we include all centre of mass relative motions of target and platform in $\underline{r}(t)$), illuminating the target with EM radiation of wavenumber k , the received signal is proportional to

$$S(k, t) = \int V(\underline{r}_o, t) \exp(2ik|\underline{r}_o - \underline{r}(t)|) d^3 r_o \quad (1)$$

If the range $r(t)$ is large compared with the spatial extent of the target then this quantity is well approximated by

$$\begin{aligned} S(k, t) &= e^{2ikr(t)} \int V(\underline{r}_o, t) \exp(-2ik\underline{k}(t) \cdot \underline{r}_o) d^3 r_o \\ &= e^{2ikr(t)} \tilde{V}(2\underline{k}(t), t) \end{aligned} \quad (2)$$

where the scattering vector $\underline{k}(t)$ is given by

$$\underline{k}(t) = k \frac{\underline{r}(t)}{|\underline{r}(t)|} \quad (3)$$

and the tilde denotes Fourier transformation:

$$\tilde{f}(\underline{k}) = \int e^{-i\underline{k} \cdot \underline{r}_o} f(\underline{r}_o) d^3 r_o \quad (4)$$

Thus the received signal can be represented as the product of a range dependent phase factor and a spatial Fourier component of the target scattering function. If the range $r(t)$ is known then the phase factor may be removed (this is the essence of standard motion compensation procedures) and the Fourier component $\tilde{V}(2\mathbf{k}(t), t)$ determined. Consequently successive returns measured at several $\underline{r}(t)$ will sample the spatial Fourier components of the target and so provide us with the raw material for the imaging of the target by inverse Fourier transformation.

The precise way in which target and platform motions select these Fourier components will be discussed in following sections of the paper. Nonetheless it is worthwhile at this point to consider the imaging process a little further.

Let us suppose that we have sampled Fourier components $\tilde{f}(\underline{k})$ of a function $f(\underline{r})$ over a limited set Z of \underline{k} vectors. We now attempt to reconstruct $f'(\underline{r})$ (as $f'(\underline{r})$) by inverse Fourier transformation.

$$f'(\underline{r}) = \frac{1}{(2\pi)^3} \int d^3k e^{i\underline{k} \cdot \underline{r}} \tilde{f}(\underline{k}) \tilde{H}_3(\underline{k}) \quad (5)$$

where

$$\tilde{H}_3(\underline{k}) = 1 \quad \underline{k} \in Z$$

$$= 0 \quad \underline{k} \notin Z$$

Substitution of (4) then gives us

$$f'(\underline{r}) = \int H_3(\underline{r} - \underline{r}') f(\underline{r}') d^3r' \quad (6)$$

where $H_3(\underline{r} - \underline{r}')$ is the point spread or imaging function given by

$$H_3(\underline{r} - \underline{r}') = \frac{1}{(2\pi)^3} \int d^3k e^{i\underline{k} \cdot (\underline{r} - \underline{r}')} \tilde{H}_3(\underline{k}) \quad (7)$$

which relates the form of the image we obtain to our ability to sample \underline{k} space. Thus, for example, if we knew $\tilde{f}(\underline{k})$ only in the plane containing vectors \underline{k}_H then we would set

$$\underline{k} = \underline{k}_H + \underline{k}_{\perp} e_{\perp}, \quad \underline{r} = \underline{r}_H + \underline{r}_{\perp} e_{\perp}$$

where \underline{e}_\perp is the unit vector perpendicular to this plane and set

$$\tilde{H}_3(\underline{k}_H + \underline{k}_\perp \underline{e}_\perp) = 1, \quad \underline{k}_\perp = 0$$

$$= 0 \quad \text{otherwise}$$

Consequently

$$H_3(\underline{r} - \underline{r}') = \frac{1}{2\pi} \delta(\underline{r}_H - \underline{r}'_H) \quad (8)$$

(a 2 dimensional delta function) and

$$f'(\underline{r}_H) = \frac{1}{2\pi} \int_{-\infty}^{\infty} d\underline{r}_\perp' f(\underline{r}_H + \underline{e}_\perp \underline{r}_\perp'), \quad (9)$$

obtaining an image which is the projection of $f(\underline{r})$ onto the plane containing the known \underline{k} vectors.

This result is of course the well known 'Fourier slice' Theorem. Should our knowledge of $\tilde{f}(\underline{k}_H)$ be restricted further in the \underline{k}_H plane

$$\begin{aligned} \tilde{H}_3(\underline{k}_H + \underline{k}_\perp \underline{e}_\perp) &= \tilde{H}_2(\underline{k}_H) \quad \underline{k}_\perp = 0 \\ &= 0 \quad \text{otherwise} \end{aligned} \quad (10)$$

then our projected image will also be defocussed:

$$f'(\underline{r}_H) = \frac{1}{2\pi} \int d^2 \underline{r}_H' H_2(\underline{r}_H - \underline{r}'_H) \int d\underline{r}_\perp' f(\underline{r}_H' + \underline{e}_\perp \underline{r}_\perp') \quad (11)$$

where

$$H_2(\underline{r}_H - \underline{r}'_H) = \frac{1}{(2\pi)^2} \int d^2 \underline{k}_H e^{i \underline{k}_H \cdot (\underline{r}_H - \underline{r}'_H)} \tilde{H}_2(\underline{k}_H) \quad (12)$$

For example knowledge of $\tilde{f}(\underline{k}_H)$ in the rectangular domain

$$k_{01} - a < k_{H1} < k_{01} + a.$$

$$k_{02} - b < k_{H2} < k_{02} + b.$$

would result in a sinc function form for H_2 :

$$H_2(\underline{r}_H - \underline{r}_{H'}) = e^{i\underline{k}_O \cdot (\underline{r}_H - \underline{r}_{H'})} \frac{\sin a(r_{H1} - r_{H1'}) \sin b(r_{H2} - r_{H2'})}{\pi^2 (r_{H1} - r_{H1'}) (r_{H2} - r_{H2'})} \quad (13)$$

In the general imaging problem \underline{k} will not be sampled in a plane but on a more complex surface determined by the platform and target motions. Nonetheless it is convenient (and consequently is customary practise) to process data (via a F.F.T. algorithm or some analogue thereof (See Appendix A)) as if it were. This will introduce further degradation of the imagery, which can be analysed as follows. Let us take the plane containing \underline{k}_H to be tangent to the surface containing the sampled \underline{k} vectors such that both surfaces contain the vector \underline{k}_O and that $\tilde{H}_2(\underline{k}_H)$ is centred around \underline{k}_O (c.f (13)). (We will see in subsequent sections that the sampled \underline{k} vectors lie on a cone like surface generated by the rotation of \underline{k}_O through relatively small angles. This readily visualised situation may help motivate the following discussion). In processing the data as if the \underline{k} vectors were coplanar we perform a 'modified Fourier inversion' of the type

$$f'(\underline{r}_H) = \frac{1}{(2\pi)^3} \int d^2k_H e^{i\underline{k}_H \cdot \underline{r}_H} \tilde{f}(\underline{k}_H + \delta\underline{k}(\underline{k}_H)) \tilde{H}_2(\underline{k}_H) \quad (14)$$

where $\delta\underline{k}(\underline{k}_H)$ is the vector correcting the approximation \underline{k}_H to the sampled \underline{k} vector to its correct value. As the support of $\tilde{H}_2(\underline{k}_H)$ is small and centred on \underline{k}_O we may expand $\delta\underline{k}$ in a Taylor series around \underline{k}_O ;

$$\delta k_\alpha = \frac{1}{2} C_{\alpha\beta\gamma} \Delta k_{H\beta} \Delta k_{H\gamma} + O(\Delta k_H^3) \quad (15)$$

Here

$$C_{\alpha\beta\gamma} = \left. \frac{\partial^2 \delta k_\alpha}{\partial \Delta k_{H\beta} \partial \Delta k_{H\gamma}} \right|_{\Delta k_H = 0} \quad (16)$$

$$\underline{k}_H = \underline{k}_O + \Delta \underline{k}_H$$

and we have used the repeated suffix tensor notation [3]. Thus we may write

$$f'(\underline{r}_H) = \frac{1}{2\pi} \int d^3r' f(\underline{r}') H_2'(\underline{r}_H, \underline{r}')$$

where

$$H_2'(\underline{r}_H, \underline{r}')$$

$$= \frac{e^{i\underline{k}_O \cdot (\underline{r}_H - \underline{r}')}}{(2\pi)^2} \int d^2 \Delta \underline{k}_H e^{i \Delta \underline{k}_H \cdot (\underline{r}_H - \underline{r}')} \quad (17)$$

$$\exp\left(-\frac{i}{2} r_{\alpha'} C_{\alpha\beta\gamma} \Delta k_H \beta \Delta k_H \gamma\right) \tilde{H}_2(\Delta \underline{k}_H)$$

This very general formula allows us to characterise the defocussing of the image due to quadratic errors in the approximation of sampled \underline{k} vectors by a planar set. In Appendix B we evaluate $H_2'(\underline{r}_H, \underline{r}')$ assuming a Gaussian model for $\tilde{H}_2(\Delta \underline{k}_H)$ [This is analytically tractable and yields readily interpretable results; a rectangular \tilde{H}_2 (cf (13)) yields results expressed in terms of Fresnel Integrals which are not as readily visualized] and demonstrate how polar format processing effects [4] arise as a simple special case of this result. In the context of SAR and ISAR imaging we expect $\delta \underline{k}$ to have a component perpendicular to the \underline{k}_H plane, specified by the curvature tensor of the surface containing the sampled \underline{k} vectors. In the following sections we will show how this can be calculated using relatively simple geometrical ideas. Furthermore it will be shown that the corruption of the image by errors in the estimation of centre of mass motion \underline{r}_H (incorrect motion compensation) may be analysed quite straightforwardly within the framework we have just presented.

The Selection of Spatial Fourier Components by Target and Platform Motions

We now return to Equation (2) and consider how target and platform motions select the spatial Fourier components of the target scattering function $V_O(\underline{r}_O, t)$ measured in a SAR or ISAR observation. We recall that all c.m relative motion is incorporated in $\underline{r}(t)$ so that the temporal variation of $V_O(\underline{r}_O, t)$ is due entirely to rotational motions of the target. Furthermore, as $\underline{k}(t)$ is of constant length (see (3)), its temporal variation can also be expressed as a rotation. Consequently, before addressing the main topic of this section, we should discuss the representation of rotations we will use in our analysis. Rotations of rigid bodies are commonly parameterised in terms of Euler's angles, particularly in the contexts of classical dynamics^[5] and the quantum theory of angular momentum^[6]. However, rotations can be described in many other ways (eg. in terms of Cayley-Klein

parameters and quaternions^[5]) and in this work we have found the axis-angle parameterisation to be particularly useful. In this case the rotation of a rigid body in three dimensions is defined by a unit vector (axis) \underline{n} , which remains unchanged by the rotation and an angle θ which defines the magnitude and direction of the rotation. This parameterisation has been discussed briefly in several discussions of the quantum theory of angular momentum^[7] but it is only recently that its utility in practical calculations has been fully recognised. A discussion of its properties is given in [2], where derivations of the results we will use are given and to which the interested reader is referred for further details.

Let us consider a vector \underline{r} , which is rotated through an angle θ around an axis \underline{n} . \underline{r} can be resolved into components parallel and perpendicular to \underline{n} , the parallel component $\underline{n}(\underline{n} \cdot \underline{r})$ remaining unchanged by the rotation. The perpendicular component $(\underline{n} \wedge \underline{r}) \wedge \underline{n}$ is transformed by the rotation into $(\underline{n} \wedge \underline{r}) \sin \theta + (\underline{n} \wedge \underline{r}) \wedge \underline{n} \cos \theta$. Consequently the rotation specified by \underline{n} , θ takes \underline{r} into \underline{r}' given by

$$\begin{aligned}\underline{r}' &= \underline{n}(\underline{n} \cdot \underline{r}) + (\underline{n} \wedge \underline{r}) \sin \theta + (\underline{n} \wedge \underline{r}) \wedge \underline{n} \cos \theta \\ &= (1 - \cos \theta) \underline{n}(\underline{n} \cdot \underline{r}) + \cos \theta \underline{r} + \sin \theta \underline{n} \wedge \underline{r}\end{aligned}\quad (18)$$

which we may express in tensor notation as

$$\underline{r}' = \underline{\mathbf{M}}(\underline{n}, \theta) \cdot \underline{r} \quad (19)$$

The Cartesian components of the dyadic $\underline{\mathbf{M}}(\underline{n}, \theta)$ are readily identified as

$$M(\underline{n}, \theta)_{\alpha\beta} = (1 - \cos \theta) n_\alpha n_\beta + \cos \theta \delta_{\alpha\beta} + \sin \theta \epsilon_{\alpha\gamma\beta} n_\gamma \quad (20)$$

where $\delta_{\alpha\beta}$ is the Kroenecker delta, n_α is a component of \underline{n} and $\epsilon_{\alpha\gamma\beta}$ is the Levi Cevita or antisymmetric tensor density^[3]. Successive rotations characterised by $(\underline{n}_1, \theta_1), (\underline{n}_2, \theta_2)$ of the vector \underline{r} then give us a vector \underline{r}''

$$\begin{aligned}\underline{r}'' &= \underline{\mathbf{M}}(\underline{n}_2, \theta_2) \cdot \underline{r}' \\ &= \underline{\mathbf{M}}(\underline{n}_2, \theta_2) \cdot \underline{\mathbf{M}}(\underline{n}_1, \theta_1) \cdot \underline{r}\end{aligned}\quad (21)$$

As is demonstrated in [2] this resultant of two rotations is equivalent to a single rotation characterised by (\underline{n}, θ) where

$$\cos \theta = \frac{1}{2}((1-c_1)(1-c_2)\Omega^2 + c_1 + c_2 + c_1c_2 - 2\Omega s_1s_2 - 1), \quad (22)$$

$$\underline{n} = C \left[(s_1s_2 + \Omega(1-c_1)(1+c_2))\underline{n}_1 + s_1s_2\Omega + (1+c_1)(1-c_2)\underline{n}_2 \right. \\ \left. + (\Omega s_2(1-c_1) + s_1(1-c_2))\underline{n}_2 \wedge \underline{n}_1 \right] \quad (23)$$

and

$$\frac{1}{C^2} = (s_1s_2 + \Omega(1-c_1)(1+c_2))^2 + (s_1s_2\Omega + (1+c_1)(1-c_2))^2 \\ + 2\Omega(s_1s_2 + \Omega(1+c_2)(1-c_1))(s_1s_2\Omega + (1+c_1)(1-c_2)) \\ + (1-\Omega^2)(\Omega s_2(1-c_1) + s_1(1-c_2))^2 \quad (24)$$

In these formulae $c_i = \cos \theta_i$, $s_i = \sin \theta_i$ ($i = 1, 2$) and $\Omega = \underline{n}_1 \cdot \underline{n}_2$, the cosine of the angle between the axes of the successive rotations. The most striking feature of these results is that the resultant of successive rotations about non parallel axes ($\underline{n}_1 \neq \underline{n}_2$) depends on the order in which the rotations are performed, that is that rotations in general do not commute

$$\underline{M}(\underline{n}_2, \theta_2) \cdot \underline{M}(\underline{n}_1, \theta_1) \neq \underline{M}(\underline{n}_1, \theta_1) \cdot \underline{M}(\underline{n}_2, \theta_2) \quad (25)$$

It is also possible to derive an equation of motion for \underline{n} , θ describing the rotation of a body subject to a time varying angular velocity $\underline{\omega}(t)$. As is discussed in [2], it can be shown that the vector $\underline{q}(t) = \theta(t) \underline{n}(t)$ satisfies the differential equation

$$\frac{dq}{dt} = \frac{(\underline{\omega} \cdot \underline{q})\underline{q}}{q^2} + \frac{1}{2} \left\{ \frac{\underline{q} \sin q}{1 - \cos q} \underline{\omega} \cdot (\underline{I} - \underline{q}\underline{q}/q^2) + \underline{\omega} \wedge \underline{q} \right\} \quad (26)$$

where \underline{I} is the unit dyadic. For small q (small rotations) we have the limiting form

$$\frac{dq}{dt} = \omega + \frac{1}{2}(\omega \wedge q) \quad (27)$$

and note [2] that this differential equation is well behaved in the vicinity of $q = 0$, which represents a zero nett rotation.

Having reviewed our rotation formalism we turn to our analysis of $\tilde{v}(2k(t), t)$. As $v(\underline{r}_o, t)$ changes only as a result of rotations of the target we may write this in terms of $v_o(\underline{r}_o)$ which specifies the spatial extent of the ship in the orientation adopted at time $t = 0$, as

$$\begin{aligned} v(\underline{r}_o, t) &= v_o (\underline{M}_s(t), \theta_o(t))^{-1} \cdot \underline{r}_o \\ &= v_o (\underline{M}_s(t)^{-1} \cdot \underline{r}_o) \end{aligned} \quad (28)$$

where $\underline{n}_s(t)$, $\theta_s(t)$ specify the rotation performed by the ship in time t . Thus we have

$$\begin{aligned} \tilde{v}(2k(t), t) &= \int d^3 r_o v_o (\underline{M}_s(t)^{-1} \cdot \underline{r}_o) e^{-2ik(t) \cdot \underline{r}_o} \\ &= \int d^3 r_o v_o(\underline{r}_o) e^{-2ik(t) \cdot \underline{M}_s(t) \cdot \underline{r}_o} \\ &= \int d^3 r_o v_o(\underline{r}_o) \exp\left(-2i(\underline{M}_s(t)^{-1} \cdot \underline{k}(t)) \cdot \underline{r}_o'\right) \end{aligned} \quad (29)$$

Here we have made the change in variables

$$\underline{M}_s(t)^{-1} \cdot \underline{r}_o \rightarrow \underline{r}_o'$$

a transformation which has unit Jacobian, and have exploited the orthogonality property of \underline{M}

$$\tilde{\underline{M}} = \underline{M}^{-1}$$

where $\tilde{\underline{M}}, \underline{M}^{-1}$ denote the transpose and inverse of \underline{M} respectively. Finally we note that, in accordance with our earlier remarks, we may set

$$\underline{k}(t) = \underline{M}_p(t) \cdot \underline{k}_o , \quad \underline{k}_o = k \frac{\underline{r}(o)}{|\underline{r}(o)|}$$

so that

$$\tilde{V}(2\underline{k}(t), t) = \tilde{v}_o \left(2 \underline{M}_s(t)^{-1} \cdot \underline{M}_p(t) \cdot \underline{k}_o \right) \quad (30)$$

showing explicitly how the target and platform motions select out spatial fourier components of the target scattering function in a fixed orientation.

SAR, ISAR and SAR/ISAR Imaging

Having shown how the target and platform motions select spatial frequency components of the target scattering function we will now apply our 'master formula' (17) to characterise SAR, ISAR and hybrid SAR/ISAR images in terms of these motions. Let us consider firstly the case where

$$\underline{M}_H(t) = \underline{M}_s(t)^{-1} \cdot \underline{M}_p(t)$$

represents a rotation around a fixed axis \underline{n} . The special cases of SAR and ISAR with uniform platform and target rotations will be covered by this analysis. Subsequently we will analyse the effect of changes in the direction of the axis of rotation during the imaging process and will then be able to address the general SAR and ISAR problems, as well as the hybrid SAR/ISAR problem. We will also consider the effects on the imagery of errors in the estimation of the centre of mass relative motion $\underline{r}(t)$ and so be able to quantify the effects of incorrect motion compensation. In this way we hope to show that all the essential features of imaging exploiting target and platform motions can be incorporated in a relatively simple and systematic conceptual and computational framework.

When a vector \underline{k}_o is rotated about an axis \underline{n} the resulting vector \underline{k} lies on a cone whose axis is \underline{n} . This basic geometrical construction is shown in Figure 1. This allows us to identify the surface on which the sampled \underline{k} vectors lie. When we now process data obtained in this way by Fourier inversion (cf(14)) we will obtain an image projected onto the plane tangent to this cone and containing \underline{k}_o . Simple vector geometry shows that this plane is normal to the vector $\underline{k}_o \wedge (\underline{n} \wedge \underline{k}_o)$. The pertinent features of the geometry of a cone lying on a tangent plane are discussed in Appendix C while in Appendix B we evaluate the tensor $C_{\alpha\beta\gamma}$ which we then substitute into our master formula (17). \underline{k}_H is now resolved into components parallel (k_{H1}) and perpendicular (k_{H2}) to \underline{k}_o and $\tilde{H}_2(k_H)$ is assumed to have the Gaussian form

$$\tilde{H}_2(\underline{k}_H) = \frac{\exp\left\{-\frac{1}{2}(\underline{k}_H - \underline{k}_O) \cdot \underline{D} \cdot (\underline{k}_H - \underline{k}_O)\right\}}{2\pi[\det \underline{D}^{-1}]^{\frac{1}{2}}} \quad (31)$$

where \underline{D} is diagonal

$$\underline{D} = \begin{pmatrix} d_1 & 0 \\ 0 & d_2 \end{pmatrix} \quad (32)$$

As is demonstrated in Appendix B this form of \underline{D} leads to an intensity point spread function with a covariance matrix given by

$$\begin{pmatrix} d_1 + \frac{c_{11}^2}{d_1} + \frac{c_{12}^2}{d_2} & c_{12}\left(\frac{c_{22}}{d_2} + \frac{c_{11}}{d_1}\right) \\ c_{12}\left(\frac{c_{22}}{d_2} + \frac{c_{11}}{d_1}\right) & d_2 + \frac{c_{22}^2}{d_2} + \frac{c_{12}^2}{d_1} \end{pmatrix} \quad (33)$$

where c_{ij} are given by

$$\begin{pmatrix} 0 & r'_2/k_O \\ r'_2 & -\frac{r'_1}{k_O} + \frac{r'_3}{k_O} \cot \Omega \end{pmatrix} \quad (34)$$

Ω being the angle between \underline{n} and \underline{k}_O .

When we identify \underline{n} with the axis of rotation of the target and the platform is assumed to be stationary (33) characterises the defocussing of an ISAR image. Conversely for a stationary target and a platform whose motions are generated by rotation around an axis \underline{n} (33) characterises a SAR image.

Let us now consider effects of the incorrect estimation of centre of mass relative motions. To do this we return to our starting point (2) and set

$$\underline{r}(t) = \underline{r}_e(t) + \delta \underline{r}(t)$$

where $\underline{r}_e(t)$ is our estimate of the centre of mass motion. If, as is reasonable in practise, we assume that

$$|\underline{r}_e(t)| \gg |\underline{r}_o(r)|, |\delta\underline{r}(t)|$$

we find that

$$k|\underline{r}_o - \underline{r}(t)| = kr_e(t) + \delta\underline{r}(t) \cdot \underline{k}_e(t) - \underline{r}_o \cdot \underline{k}_e(t)$$

where

$$\underline{k}_e(t) = k \frac{\underline{r}_e(t)}{|\underline{r}_e(t)|},$$

$\delta\underline{r}(t)$ may now be decomposed into a gross error $\delta\bar{r}$ and time varying parts due to errors in the estimation of centre of mass velocity and acceleration respectively

$$\delta\underline{r}(t) = \delta\bar{r} + \underline{v}t + \frac{1}{2}\underline{a}t^2$$

Substitution into (1) then give us

$$\begin{aligned} S(k, t) &= e^{2ikr_e(t)} e^{2i\delta\bar{r} \cdot \underline{k}_e(t)} e^{2ity \cdot \underline{k}_e(t)} \\ &\times e^{it^2 \underline{a} \cdot \underline{k}_e(t)} \int d^3 \underline{r}_o e^{-2ik\underline{k}_e(t) \cdot \underline{r}_o} v(\underline{r}_o, t) \\ &- e^{2ikr_e(t)} e^{2i\delta\bar{r} \cdot \underline{k}_e(t)} e^{2ity \cdot \underline{k}_e(t)} \\ &\times e^{it^2 \underline{a} \cdot \underline{k}_e(t)} \tilde{v}_o(2\underline{M}_H(t) \cdot \underline{k}_{eo}) \end{aligned} \quad (35)$$

where $\underline{M}_H(t) = \underline{M}_S(t)^{-1} \cdot \underline{M}_P(t)$.

Consequently Fourier inversion of data sampled with an incorrect estimate of $\underline{r}(t)$ will yield an image of the form:

$$\begin{aligned}
I'(\underline{x}_H) &= \frac{1}{2\pi} \int d^3r' v_O(\underline{r}') \\
&\times \frac{e^{ik_O \cdot (\underline{x}_H - \underline{x}_{H'} - \delta \underline{r})}}{(2\pi)^2} \int d^2k_H e^{+ik_H \cdot (\underline{x}_H + \delta \underline{r}' + \frac{\underline{v} \cdot \underline{k}_O (\underline{n} \wedge \underline{k}_O)}{\omega |\underline{n} \wedge \underline{k}_O|^2} - \underline{x}_{H'})} \\
&\left(x e^{i\underline{v} \cdot \underline{k}_H \left[\frac{\underline{k}_H \cdot (\underline{n} \wedge \underline{k}_O)}{\omega |\underline{n} \wedge \underline{k}_O|^2} \right]} e^{\frac{i\alpha \cdot \underline{k}_O}{2} \left[\frac{\underline{k}_H \cdot (\underline{n} \wedge \underline{k}_O)}{\omega |\underline{n} \wedge \underline{k}_O|^2} \right]^2} \right) \\
&\times e^{-\frac{i}{2} r_{\alpha'} C_{\alpha\beta\gamma} k_{H\alpha} k_{H\beta} \tilde{H}_2(\underline{k}_H)}
\end{aligned} \tag{36}$$

where we have used

$$t = \underline{k}_H \cdot (\underline{n} \wedge \underline{k}_O) / \omega |\underline{n} \wedge \underline{k}_O|^2 + O(\underline{k}_H)^3$$

The effect of the linear phase shift within the integral over \underline{k}_H is to shift the argument of the imaging function

$$\underline{x}_H - \underline{x}_{H'} \rightarrow \underline{x}_H + \delta \underline{r}' + \frac{\underline{v} \cdot \underline{k}_O (\underline{n} \wedge \underline{k}_O)}{\omega |\underline{n} \wedge \underline{k}_O|^2} - \underline{x}_{H'} \tag{37}$$

inducing a shift in the image of the target, proportional to the radial component of \underline{v} and in the direction of $\underline{n} \wedge \underline{k}_O$. In the standard SAR case this shift is in the 'along track' direction while in the ISAR case the familiar

$$\omega \delta r \quad \alpha \quad v$$

relationship is in evidence. The quadratic phase correction terms induce a further defocussing of the image; unlike the 'curvature' defocussing we have just discussed this defocussing depends only on the experimental geometry and the errors in c.m estimation \underline{y} , \underline{a} and not on the spatial extent of the target. Reference to Appendix B allows us to obtain a quantitative estimate of these defocussing effects through (17).

We now consider the effect of changes in the direction of the axis generating the rotation of the \underline{k} vectors within the time during which we form the image. This will bring about a further contribution to $\delta k(k_H)$ which will not in general be perpendicular to the imaging plane. In our discussion of defocussing effects we need only consider contributions to δk which are of order (Δk_H^2) . From (29) we see that $\underline{q} = \underline{n}\theta$ satisfies the differential equation

$$\frac{d\underline{q}}{dt} - \underline{\omega}(t) + \frac{1}{2}\underline{\omega}(t) \wedge \underline{q} \quad (38)$$

in the limit of small \underline{q} (sufficient for our purposes) where the angular velocity varies in direction as well as magnitude. Thus we write

$$\underline{\omega}(t) = \omega_0(t) \underline{n} + \underline{\omega}_1(t) \quad (39)$$

where

$$\underline{n} \cdot \underline{\omega}_1(t) = 0$$

and \underline{n} is a fixed direction.

Finally we set

$$\theta_0(t) = \int_0^t \omega_0(t') dt'$$

and write

$$\begin{aligned} \underline{q}(t) &= \theta_0(t) \underline{n} + \delta \underline{q}(t) \\ &= \underline{q}_0(t) + \delta \underline{q}(t) \end{aligned}$$

Substitution into (29) then gives

$$\frac{d}{dt} \delta g(t) = \underline{\omega}(t) + \frac{1}{2} \omega_0(t) \underline{n} \wedge \delta g(t) + \underline{\omega}(t) \wedge [g_0(t) + \delta g(t)] \quad (40)$$

which has, to lowest order in $\underline{\omega}_1(t)$, the solution

$$\delta g(t) = \int_0^t \underline{\omega}_1(t') dt' + \frac{1}{2} \int_0^t \underline{\omega}_1(t') \wedge g_0(t') dt' \quad (41)$$

so that

$$g(t) = \theta_0(t) \underline{n} + \int_0^t \underline{\omega}_1(t') dt' + \frac{1}{2} \int_0^t \theta_0(t') \underline{\omega}_1(t') dt' \wedge \underline{n} \quad (42)$$

We note that the second and third terms in (45) are orthogonal to \underline{n} . Consequently, if we retain only those terms which are linear in $\underline{\omega}_1(t)$ we see that

$$\theta(t) = \theta_0(t).$$

$$\underline{n}(t) = \underline{n} + \frac{1}{\theta_0(t)} \left[\int_0^t \underline{\omega}_1(t') dt' + \frac{1}{2} \int_0^t \theta_0(t') \underline{\omega}_1(t') dt' \wedge \underline{n} \right]$$

$$= \underline{n} + \delta \underline{n}(t).$$

Thus, at some time t , the vector \underline{k}_0 will have been rotated into $\underline{k}'(t)$, given by

$$\begin{aligned} \underline{k}'(t) &= (1 - \cos \theta_0(t)) (\underline{n} + \delta \underline{n}) \cdot \underline{k}_0 (\underline{n} + \delta \underline{n}) + \cos \theta_0(t) \underline{k}_0 \\ &\quad + \sin \theta_0(t) (\underline{n} + \delta \underline{n}) \wedge \underline{k}_0 \end{aligned} \quad (43)$$

The corresponding vector $\underline{k}(t)$ obtained by a rotation of \underline{k}_0 through $\theta_0(t)$ about the unperturbed axis is

$$\underline{k}(t) = [1 - \cos \theta_0(t)] (\underline{n} \cdot \underline{k}_0) \underline{n} + \cos \theta_0(t) \underline{k}_0 + \sin \theta_0(t) \underline{n} \wedge \underline{k}_0 \quad (44)$$

The change in \underline{k} due to the perturbation of the axis of rotation is given by

$$\begin{aligned}\underline{k}'(t) - \underline{k}(t) = & [1 - \cos\theta_O(t)]((\delta\underline{n} \cdot \underline{k}_O)\underline{n} + (\underline{n} \cdot \underline{k}_O)\delta\underline{n}) \\ & + \sin\theta_O(t)\delta\underline{n} \wedge \underline{k}_O\end{aligned}\quad (45)$$

with which we must supplement $\delta\underline{k}$ to identify the corresponding defocussing effects. We must now evaluate $\delta\underline{r}(t)$ in terms of $\theta_O(t)$; to do this we must postulate forms of $\omega_O(t)$, $\underline{\omega}_1(t)$. For short times we set

$$\begin{aligned}\omega_O(r) &= \omega_O \\ \underline{\omega}_1(t) &= \omega_1 t \quad \hat{\underline{\omega}}_1\end{aligned}\quad (46)$$

so that

$$\delta\underline{n} = \frac{\omega_1}{2\omega_O^2} \left[\theta \hat{\underline{\omega}}_1 + \frac{1}{3} \theta^2 \hat{\underline{\omega}}_1 \wedge \underline{n} \right] \quad (47)$$

From Appendix C we see that

$$\theta \sim \frac{\Delta k_H \cdot (\underline{n} \wedge \underline{k}_O)}{|\underline{n} \wedge \underline{k}_O|^2} \quad (48)$$

so that ultimately we have

$$\underline{k}'(t) - \underline{k}(t) = \frac{\omega_1}{2\omega_O^2} \frac{[\Delta k_H \cdot (\underline{n} \wedge \underline{k}_O)]^2}{|\underline{n} \wedge \underline{k}_O|^4} \hat{\underline{\omega}}_1 \wedge \underline{k}_O \quad (49)$$

with which we supplement (17) to yield

$$H_2'(\underline{r}_H, \underline{r}') = e^{-i\underline{k}_O \cdot (\underline{r}_H - \underline{r}'_H)}$$

$$\times \int d^2 \underline{k}_H e^{-i \underline{k}_H \cdot (\underline{r}_H - \underline{r}'_H)} H'_2(\underline{k}_H)$$

$$\exp \left\{ - \frac{i r_\alpha'}{2} C_{\alpha\beta\gamma} k_H \beta k_{H\gamma} \right.$$

$$\left. - \frac{i}{2} \frac{[\underline{k}_H \cdot (\underline{n} \wedge \underline{k}_O)]^2}{| \underline{n} \wedge \underline{k}_O |^2} \frac{\omega_1}{\omega_0^2} \frac{\underline{r}' \cdot (\hat{\omega}_1 \wedge \underline{k}_O)}{| \underline{n} \wedge \underline{k}_O |^2} \right\} \quad (50)$$

Comparison with the analysis in Appendix B shows that the effect of variation in the direction of the axis of rotation merely supplements the c_{22} element of \underline{C} by a factor

$$+ \frac{\omega_1}{\omega_0^2} \frac{\underline{r}' \cdot (\hat{\omega}_1 \wedge \underline{k}_O)}{| \underline{n} \wedge \underline{k}_O |^2}$$

Hybrid SAR/ISAR in which both the target and platform have motions provides an interesting case in which the direction of the axis of rotation varies with time. Rotations about non-parallel axes do not commute and, as a consequence of this, the direction of the axis specifying the resultant of two such rotations will vary in time. Specifically, if the rotation of the target is specified by axis, angle variables

$$\theta_S(t), \underline{n}_S(t)$$

while

$$\theta_p(t), \underline{n}_p(t)$$

specify the rotation of the platform then $\theta(t), \underline{n}(t)$ specifying the resultant rotation satisfy

$$\underline{n}(t) \theta(t) = -\theta_s(t) \underline{n}(t) + \theta_p(t) \underline{n}_p(t) - \frac{1}{2} \theta_s(t) \theta_p(t) \underline{n}_s(t) \wedge \underline{n}_p(t) + O(\theta^3) \quad (51)$$

If now we set

$$\theta_s(t) \underline{n}_s(t) = \hat{\omega}_s \omega_s t$$

$$\theta_p(t) \underline{n}_p(t) = \hat{\omega}_p \omega_p t$$

then

$$\theta(t) \underline{n}(t) = -\omega_s \hat{\omega}_s t + \omega_p \hat{\omega}_p t - \frac{1}{2} \omega_s \omega_p t^2 \hat{\omega}_s \wedge \hat{\omega}_p + O(t^3) \quad (52)$$

comparison with (39) then allows us to make the identifications

$$\underline{\omega}_0 = \omega_p \hat{\omega}_p - \omega_s \hat{\omega}_s$$

$$\underline{\omega}_1 = \omega_s \omega_p t \hat{\omega}_s \wedge \hat{\omega}_p$$

noting that $\underline{\omega}_1$ is indeed perpendicular to $\underline{\omega}_0$, as required in our analysis. Consequently we see that the non commutativity of rotations leads to an extra source of defocussing in hybrid SAR/ISAR imaging, which, as we have seen, can be accommodated quite straightforwardly in our formal framework.

Point Target Simulations

In this section an initial verification of the theory from the previous sections is provided by comparing the effect of mismatched processing on the predicted and actual sizes and shapes of the image of a point target. The mismatch introduced is simply that which results in normal practise from a lack of knowledge of the target rotation rate and from the requirement to produce a two dimensional image from three dimensional \underline{k} vector samples.

Two examples are chosen as indicated in Figure 2. In both cases a target is viewed at a low grazing angle by a stationary radar. The target is rotated with a constant rotation vector $\underline{\omega}$. In case one (Figure 2a) $\underline{\omega}$ is vertical, corresponding to a yaw motion of a ship. In case two (Figure 2b) $\underline{\omega}$ is 45° from the vertical, in the plane containing the radar line of sight and the vertical direction. A number of individual point scatterers are positioned on the target in each case, as shown in Figure 2. The radar parameters adopted in the simulations are listed below the figure.

It is assumed that the radar has a wide instantaneous bandwidth, so that a range profile may be derived for each angular position of the target. The rotation vector is assumed to be unknown, so that range and Doppler migration cannot be corrected effectively prior to image formation. The image is therefore derived by simple Fourier transformation of a time sequence of radar returns in each range cell of the range profile. The processing is (as is shown in Appendix A) analogous to assuming that the measured \underline{k} vector samples come from a rectilinear two dimensional grid on a plane in \underline{k} space. As we have seen in our previous discussion \underline{k} vectors are sampled from the surface of a cone (providing the rotation vector $\underline{\omega}$ does not change direction during the imaging process) and the projection plane is tangent to this cone. In Appendix B it is shown that the errors $\delta \underline{k}$ in the rectangular grid processing described above lead to a distortion of the target point spread function such that

$$\langle x^2 \rangle = d_1 + \frac{r_2'^2}{k_o^2 d_2} \quad (53)$$

$$\langle y^2 \rangle = d_2 + \frac{(r_1' - r_3' \cot \Omega)^2}{k_o^2 d_2} + \frac{r_2'^2}{k_o^2 d_1} \quad (54)$$

$$\langle xy \rangle = - \frac{r_2' (r_1' - r_3' \cot \Omega)}{k_o^2 d_2} \quad (55)$$

where r_1' , r_2' , r_3' are the position coordinates of the scatterer relative to the rotation origin and d_1, d_2 , Ω and k_0 are as defined in Appendix B. Figures 3, 4, 5 and 6 show the point spread functions (PSF) derived by simulation of the rotation and radar processing of the various scatterers in the two cases illustrated in Figure 2. Table 1 compares the moments of the PSF with (53), (54) and (55). The excellent agreement obtained indicates that the approximations made in our analysis are sufficient to provide an accurate representation of the imaging process.

It is worth considering whether the results obtained from the formal analysis used here can be predicted by the ad hoc methods customarily employed in the description of ISAR. Figure 3 shows the PSF for a target at the origin in case 1. A scatterer offset in x (along the line of sight (LOS)) undergoes Doppler migration in Range Doppler processing; this explains the additional spread in y in figure 4(b). A scatterer offset in y (perpendicular to both LOS and the rotation vector) undergoes Range migration, which both produces a spread in x and reduces the time in each range cell. This in turn produces a spread in the Doppler domain y and so explains Figure 4(a). The spreading of a point offset in both x and y is more difficult, if not impossible, to derive (or rationalise post hoc) in this way.

In case 2 the rotation vector ω is not perpendicular to the LOS. The usual ISAR analysis of this case considers only the projection of ω onto the plane perpendicular to LOS. This ad hoc method correctly predicts the image resolution of points offset in directions perpendicular to the projection of ω (x or y in our figure) but fails to predict a mismatch for scatterers offset along the direction of projection of ω (ie. in z). A mismatch does occur, however, as illustrated in Figure 4(d) and is correctly described by the formal methods used here. This simple example demonstrates the dangers of analysing ISAR from the starting point of Range-Doppler processing, subject to progressive corrections applied ad hoc, and the ease with which our formalism encompasses cases for which the conventional analysis is either too complex or incorrect.

Conclusions

In this report we have introduced a theoretical framework within which it is possible to analyse the effects of simultaneous target and platform motions on SAR and ISAR processing techniques, by unifying both within the hybrid SAR/ISAR process. Although our formalism is general and of widespread potential utility, we have shown that it is readily applied to practical SAR and ISAR situations which, from the standard Range-Doppler imaging standpoint, are difficult if not impossible to analyse correctly. Two such special cases have been simulated on the computer, with results which are in excellent agreement with the predictions of our analysis.

While the work reported here is necessarily of a preliminary nature we feel that the approach we have developed has already demonstrated its practical applicability and that it has the potential to make tractable many unresolved problems occurring in the imaging of maritime targets.

APPENDIX A

In this appendix we establish the connection between standard SAR and ISAR processing and our \underline{k} space imaging formalism. The conventional description of ISAR processing starts with a high range resolution radar of bandwidth B recording a set of range profiles with range resolution $\ell_r = 2B/c$. If the target is rotating each scatterer on the target is moving with respect to the radar with a range rate v_r proportional to its distance from the target's centre of rotation, measured perpendicular to the radar line of sight \underline{r}_o and the rotation vector $\underline{\omega}$ ie.

$$v_r = (\underline{\omega} \wedge \underline{r}) \cdot \hat{\underline{r}}_o = (\hat{\underline{r}}_o \wedge \underline{\omega}) \cdot \underline{r} \quad (A.1)$$

where \underline{r} is the position vector of the scatterer. The Doppler frequency f_d of the scatterer is given by

$$f_d = \frac{2v_r}{\lambda} = \frac{2f_o}{c} (\hat{\underline{r}}_o \wedge \underline{\omega}) \cdot \underline{r} \quad (A.2)$$

Thus, for a small rotation angle, a frequency analysis of the signal in each range cell produces an output at each frequency f corresponding to all scatterers at a distance $f_c/(2f_o \hat{\underline{r}}_o \wedge \underline{\omega})$ from the centre of rotation, measured in the direction $(\hat{\underline{r}}_o \wedge \underline{\omega})$. The across range resolution ℓ_a is given by

$$\ell_a = \frac{c}{2(f_o \hat{\underline{r}}_o \wedge \underline{\omega} \delta t)} \quad (A.3)$$

On converting this description to spatial frequency \underline{k} we find that, for small angles of rotation, $\hat{\underline{V}}(\underline{k})$ is measured in a plane perpendicular to $(\underline{\omega} \wedge \underline{r}_o) \wedge \underline{r}_o$ over an interval δk_r in the direction $\hat{\underline{r}}_o$ and δk_a in the direction $\underline{\omega} \wedge \hat{\underline{r}}_o$ where

$$\delta k_r = \frac{4\pi B}{c} \quad (A.4)$$

$$\delta k_a = k_o \hat{\underline{r}}_o \wedge \underline{\omega} \delta t$$

From the Fourier transform relation $\delta K = 2\pi/\ell$ we find that the equations for ℓ_r , ℓ_a are equivalent to those for δK_r , δK_a .

For SAR range resolution is identical to ISAR. Across range resolution is, however, derived by integrating the returns from a sideways looking radar mounted on a moving platform. For an airborne radar, travelling at velocity v perpendicular to the radar line of sight at a range R from the target, the rate of change of angle of view θ at the target is given by

$$\frac{d\theta}{dt} = \frac{v}{R}$$

(A.5)

The usual method of processing SAR data is to correlate the received signal from each range cell with a linear FM waveform. This is equivalent to firstly correcting the phase of the signal for the change of range between the radar and secondly performing a Fourier transform. By comparing the Fourier transform to the frequency analysis of ISAR processing and equating $\frac{d\theta}{dt}$ (A.5) to ω in ISAR, one shows that the SAR and ISAR processes are essentially the same, the only difference being that in ISAR the rotation is performed by the target while in SAR it comes from the platform motion. The connection with k space processing for SAR is therefore quite analogous with that for ISAR discussed above.

APPENDIX B

In this appendix we evaluate the master formula (17) assuming $\tilde{H}_2(\underline{k}_H)$ is represented by the Gaussian function

$$\tilde{H}_2(\underline{k}_H) = \frac{\exp\left\{-\frac{1}{2}(\underline{k}_H - \underline{k}_O) \cdot \underline{D} \cdot (\underline{k}_H - \underline{k}_O)\right\}}{2\pi[\det \underline{D}^{-1}]^{\frac{1}{2}}} \quad (B.1)$$

where

$$\underline{D} = \begin{pmatrix} d_{11} & d_{12} \\ d_{21} & d_{22} \end{pmatrix} \quad (B.2)$$

and that (c.f 17)

$$\delta \underline{k} \cdot \underline{r}' = \frac{1}{2}(\underline{k}_H - \underline{k}_O) \cdot \underline{C} \cdot (\underline{k}_H - \underline{k}_O) \quad (B.3)$$

where

$$\underline{C} = \begin{pmatrix} c_{11} & c_{12} \\ c_{21} & c_{22} \end{pmatrix} \quad (B.4)$$

Consequently

$$\begin{aligned} H_2'(\underline{x}_H, \underline{x}') &= \frac{e^{i\underline{k}_O \cdot (\underline{x}_H - \underline{x}'_H)}}{(2\pi)^3 \det \underline{D}^{-1}^{\frac{1}{2}}} \int d^2 k_H e^{i\underline{k}_H \cdot (\underline{x}_H - \underline{x}'_H)} \\ &\quad \exp\left[-\frac{1}{2}\tilde{\underline{k}}_H \cdot (\underline{D} + i\underline{C}) \cdot \underline{k}_H\right] \end{aligned} \quad (B.5)$$

We now focus our attention on the integral

$$\int d^2 k_H e^{i\underline{k}_H \cdot \underline{R}} \exp\left[-\frac{1}{2}\tilde{\underline{k}}_H \cdot \underline{Z} \cdot \underline{k}_H\right]$$

where $\underline{R} = \underline{\xi}_H - \underline{\xi}_H'$ and $\underline{Z} = \underline{D} + i\underline{C}$

This has the value

$$\frac{2\pi}{(\det \underline{Z})^{\frac{1}{2}}} \exp \left\{ - \frac{1}{2} \tilde{\underline{R}} \cdot \underline{Z}^{-1} \cdot \underline{R} \right\} \quad (\text{B.6})$$

where

$$\underline{Z}^{-1} = \text{Adj} \frac{\underline{Z}}{(\det \underline{Z})}$$

In the special case of 2×2 matrices the following identities hold:

$$\text{Adj}(\underline{D} + i\underline{C}) = \text{Adj} \underline{D} + i \text{Adj} \underline{C},$$

$$\det(\underline{D} + i\underline{C}) = \det \underline{D} - \det \underline{C} + i \underline{D} \odot \underline{C}$$

where

$$\underline{D} \odot \underline{C} = c_{22}d_{11} + c_{11}d_{22} - c_{12}d_{21} - c_{21}d_{12}$$

and

$$\underline{D} \cdot \text{Adj} \underline{C} + \underline{C} \cdot \text{Adj} \underline{D} = \underline{D} \odot \underline{C} \begin{pmatrix} 1 & 0 \\ 0 & 1 \end{pmatrix}$$

Consequently, if we set

$$\det \underline{D} = \alpha, \det \underline{C} = \beta, \underline{D} \odot \underline{C} = \gamma \quad (\text{B.10})$$

we may write

$$\underline{z}^{-1} = \frac{\text{Adj } \underline{D} + i \text{Adj } \underline{\underline{C}}}{(\alpha - \beta + i\gamma)}$$

(B.11)

$$= \frac{((\alpha - \beta) \text{Adj } \underline{D} + \gamma \text{Adj } \underline{\underline{C}}) + i((\alpha - \beta) \text{Adj } \underline{\underline{C}} - \gamma \text{Adj } \underline{D})}{((\alpha - \beta)^2 + \gamma^2)}$$

so that

$$\int d^2 k_H e^{ik_H \cdot R} \exp\left(-\frac{1}{2} \tilde{k}_H \cdot z \cdot k_H\right)$$

$$= \frac{2\pi}{[(\alpha - \beta) + \gamma^2]^{\frac{1}{4}}} \exp\left[-\frac{i}{2} \tan^{-1}\left(\frac{\gamma}{\alpha - \beta}\right)\right]$$

$$x \exp\left\{-\frac{1}{2} \frac{[(\alpha - \beta) \tilde{R} \cdot \text{Adj } \underline{D} \cdot R + \gamma \tilde{R} \cdot \text{Adj } \underline{\underline{C}} \cdot \underline{R}]}{[(\alpha - \beta)^2 + \gamma^2]}\right\} \quad (\text{B.12})$$

$$x \exp\left\{-\frac{i}{2} \frac{[(\alpha - \beta) \tilde{R} \cdot \text{Adj } \underline{\underline{C}} \cdot R - \gamma \tilde{R} \cdot \text{Adj } \underline{D} \cdot R]}{[(\alpha - \beta)^2 + \gamma^2]}\right\}$$

where we have explicitly separated the expression into amplitude and phase factors. While the phase term may be of importance in future work, particularly with reference to the interference patterns which occur in defocussed images of complex targets, we will restrict our attention here to a more detailed discussion of the amplitude factor. To simplify the formulae we make the assumption that \underline{D} is diagonal (the 1 or x direction being along k_o , the 2 or y direction being along $n \wedge k_o$)

$$\text{ie } \underline{D} = \begin{pmatrix} d_1 & 0 \\ 0 & d_2 \end{pmatrix}$$

while \underline{C} is symmetric and takes the form

$$\underline{C} = \begin{pmatrix} c_{11} & c_{12} \\ c_{12} & c_{22} \end{pmatrix}.$$

α , β , and γ can now be evaluated as

$$\alpha = d_1 d_2$$

$$\beta = c_{22} c_{11} - c_{12}^2$$

$$\gamma = d_{11} c_{22} + d_{22} c_{11}$$

The amplitude point spread function now takes the form of a Gaussian

$$\exp \left\{ -\frac{1}{2} \tilde{R} \cdot \underline{A} \cdot \underline{R} \right\} \quad (\text{B.13})$$

where

$$\underline{A} = \begin{pmatrix} \frac{(\alpha-\beta)d_2 + \gamma c_{22}}{(\alpha-\beta)^2 + \gamma^2} & \frac{-\gamma c_{12}}{(\alpha-\beta)^2 + \gamma^2} \\ \frac{-\gamma c_{12}}{(\alpha-\beta)^2 + \gamma^2} & \frac{(\alpha-\beta)d_1 + \gamma c_{11}}{(\alpha-\beta)^2 + \gamma^2} \end{pmatrix} \quad (\text{B.14})$$

The covariance matrix of the point spread function, which gives a quantitative measure of the defocussing, is given by the inverse of A , which takes the relatively simple form

$$\underline{A}^{-1} = \begin{pmatrix} d_1 + \frac{c_{11}^2}{d_1} + \frac{c_{12}^2}{d_2} & c_{12} \left(\frac{c_{22}}{d_1} + \frac{c_{11}}{d_1} \right) \\ c_{12} \left(\frac{c_{22}}{d_2} + \frac{c_{11}}{d_1} \right) & d_2 + \left(\frac{c_{22}^2}{d_2} + \frac{c_{12}^2}{d_1} \right) \end{pmatrix} \quad (\text{B.15})$$

This result forms the basis our interpretation of the simulation results in the body of the text. It now remains to evaluate the C matrix in a couple of special cases of practical importance. To make contact with our simulation work we consider the set of k vectors generated by the rotation of a vector k around an axis n. The magnitude of k varies with the frequency cycle of the transmitted signal. Imaging is carried out by Fourier transformation in the plane normal to $\underline{k}_o \wedge (\underline{n} \wedge \underline{k}_o)$. A given k vector, of magnitude k_t and direction obtained by a rotation of γ about n from that of \underline{k}_o , can be resolved into components (1,2,3) parallel to $(\underline{k}_o, \underline{n} \wedge \underline{k}_o, \underline{k}_o \wedge (\underline{n} \wedge \underline{k}_o))$ as

$$\underline{k} = (k_t (\cos^2 \Omega + \cos \theta \sin^2 \Omega), k_t \sin \Omega \sin \theta, k_t (1 - \cos \theta) \cos \Omega \sin \Omega), \quad (B.16)$$

$$\text{where } \cos \Omega = \frac{\underline{n} \cdot \underline{k}_o}{k_o}.$$

This vector is approximated in the transform plane by

$$\underline{k}_H = (k_t, \theta k_o \sin \Omega, 0) \quad (B.17)$$

so that we may write

$$\begin{aligned} \delta \underline{k} &= (k_t \sin^2 \Omega (\cos \theta - 1), (k_t \sin \theta - k_o \theta) \sin \Omega, \\ &\quad k_t (1 - \cos \theta) \sin \Omega \cos \Omega) \end{aligned} \quad (B.18)$$

Elements of the tensor $C_{\alpha\beta\gamma}$ may now be obtained by differentiation with respect to $(\underline{k}_H)_1 = k_t$ and $(\underline{k}_H)_2 = \theta k_o \sin \Omega$ and setting $k_t = k_o$, $\theta = 0$. In this way we evaluate the C matrix as

$$C = \begin{pmatrix} 0 & \frac{r'_2}{k_o} & 0 \\ \frac{r'_2}{k_o} & \frac{-r'_1}{k_o} + \frac{r'_3 \cot \Omega}{k_o} & 0 \end{pmatrix}, \quad (B.19)$$

remembering that Ω is the angle between \underline{k}_o and n, so that the covariance matrix takes the form

$$A^{-1} = \begin{pmatrix} d_1 + \frac{r'_2}{k_o^2 d_2} & -\frac{r'_2}{k_o^2 d_2} (r'_1 - r'_3 \cot \Omega) \\ -\frac{r'_2}{k_o^2 d_2} (r'_1 - r'_3 \cot \Omega) & d_2 + \frac{(r'_1 - r'_3 \cot \Omega)^2}{k_o^2 d_2} + \frac{r'^2_2}{k_o^2 d_1} \end{pmatrix}$$

The result appropriate to polar format defocussing is obtained by setting $\cot \Omega = 0$.

APPENDIX C

In this appendix we will examine those features of the geometry of a cone lying on a tangent plane which are required in our analysis of SAR and ISAR imaging. In particular we will show how to relate the component of a vector lying on the cone resolved onto the tangent plane to its component perpendicular to the plane and so derive an expression for the curvature of the cone. Sufficient detail to illustrate the methods of calculation, consistent with the requirement of reasonable brevity, will be presented.

Consider a vector \underline{k}_o rotated through an angle θ about an axis \underline{n}_o into the vector \underline{k} , lying on the cone shown in Figure 1. Simple vector analysis shows that the vector $\underline{k}_o \wedge (\underline{n}_o \wedge \underline{k}_o)$ is normal to the plane tangent to the cone and containing \underline{k}_o ; the unit vector normal to this plane is given by

$$\hat{\underline{e}}_{\perp} = \frac{\underline{n} - \hat{\underline{k}}_o \psi}{(1 - \psi^2)^{\frac{1}{2}}} \quad (C.1)$$

where $\hat{\underline{k}}_o = \frac{\underline{k}_o}{|\underline{k}_o|}$ and $\psi = \underline{k}_o \cdot \underline{n}_o$, the cosine of the angle between \underline{k}_o , \underline{n}_o .

From (18) we see that

$$\underline{k} = k((1 - \cos\theta)\psi\underline{n} + \cos\theta\hat{\underline{k}}_o + \sin\theta\underline{n}_o \wedge \hat{\underline{k}}_o) \quad (C.2)$$

and so

$$\underline{e}_{\perp} \cdot \underline{k}_o = k\psi(1 - \cos\theta)(1 - \psi^2)^{\frac{1}{2}}; \quad (C.3)$$

the component of \underline{k} resolved onto the tangent plane is then given by

$$\underline{k}_H = \underline{k} - \underline{e}_{\perp} = (\psi^2 + (1 - \psi^2)\cos\theta)\underline{k}_o + \sin\theta\underline{n} \wedge \underline{k}_o \quad (C.4)$$

We now consider the inverse of this problem; given a vector \underline{g}_H lying in the tangent plane, what is the corresponding \underline{g}_{\perp} so that $\underline{g} = \underline{g}_H + \underline{g}_{\perp}$ lies on the cone. \underline{g}_H is resolved into components within the tangent plane parallel and perpendicular to $\hat{\underline{k}}_o$ given by

$$\alpha = \underline{g}_H \cdot \hat{\underline{k}}_O$$

$$\beta = \underline{g}_H \cdot \frac{(\hat{\underline{k}}_O \wedge \underline{n}_O)}{(1 - \psi^2)^{\frac{1}{2}}} \quad (C.5)$$

These equations can now be solved for θ , the angle which rotates $\underline{q}\hat{\underline{k}}_O$ into \underline{g} . From (C.5) we see that

$$\begin{aligned} \alpha &= q(\psi^2 + (1 - \psi^2)\cos\theta) \\ \beta &= -q\sin\theta(1 - \psi^2)^{\frac{1}{2}} \end{aligned} \quad (C.6)$$

Now on introducing $\beta/\alpha = \eta$ we find that θ satisfies

$$\frac{1 - s^2}{s^2} + \cos\theta = -\frac{1}{\eta s} \sin\theta \quad (C.7)$$

where $s^2 = 1 - \psi^2$.

To solve this we make the substitution $\zeta = e^{i\theta}$ which converts (C.7) into the quadratic equation

$$\zeta^2 \left(1 - \frac{i}{\eta s}\right) + 2\zeta \frac{(1 - s^2)}{s^2} + \left(1 + \frac{i}{\eta s}\right) = 0 \quad (C.8)$$

whose solutions are

$$\zeta = \frac{-\frac{(1 - s^2)}{s^2} \pm \sqrt{\frac{(1 - s^2)^2}{s^4} - \left(1 + \frac{1}{\eta^2 s^2}\right)}}{\left(1 - \frac{i}{\eta s}\right)} \quad (C.9)$$

We see that as long as

$$1 + \frac{1}{\eta^2 s^2} > \frac{(1 - s^2)^2}{s^4} \quad (C.10)$$

$|\zeta| = 1$ and θ is real. Geometrically this corresponds to the condition that \underline{g}_H is under the cone. To identify the appropriate root of the quadratic equation we let \underline{g}_H become collinear with $\hat{\underline{k}}_O$. Then $\beta \rightarrow 0$, $\eta \rightarrow 0$ and

$$\zeta = \pm \frac{i/\eta s}{-i/\eta s};$$

for $\zeta = 1$ as $\theta = 0$ we chose the root

$$\zeta = -\frac{\left(\frac{1-s^2}{s^2} + i \left(1 + \frac{1}{\eta^2 s^2} \right) - \frac{(1-s^2)^2}{s^4} \right)^{\frac{1}{2}}}{\left(1 - \frac{i}{\eta s} \right)} \quad (C.11)$$

From this we see that

$$\theta = \pi + \phi_1 - \phi_2 \quad (C.12)$$

where

$$\phi_1 = \tan^{-1} \left\{ \frac{s^2}{(1-s^2)^2} (s^2 + \eta^2) - 1 \right\}^{\frac{1}{2}} \quad (C.13)$$

$$\phi_2 = \tan^{-1} \left(-\frac{1}{\eta s} \right)$$

and

$$-\pi/2 < \phi_1, \phi_2 < \pi/2.$$

Having found θ , q is given by

$$q = \frac{\alpha}{(\psi^2 + (1-\psi^2)\cos\theta)} \quad (C.14)$$

so that

$$q_{\perp} = \frac{\alpha\psi(1-\cos\theta)}{(\psi^2 + (1-\psi^2)\cos\theta)} (\underline{n}_0 - \hat{\psi}\underline{k}_0) \quad (C.15)$$

While it is possible to express $\cos \theta$ in terms of ψ, η the resulting expressions are cumbersome and of little practical use and consequently are omitted.

We now require an expression analogous to (15) for g_H close to \hat{k}_o . This can be obtained by direct expansion of the results we have just obtained. In outline, we set

$$\alpha = k_o - \delta q_1$$

$$\beta = \delta q_2$$

so that

$$\eta = \frac{\delta q_2}{k_o - \delta q_1}$$

and find to lowest order in $\delta q_1, \delta q_2$

$$\phi_1 \sim \frac{\pi}{2} - \frac{\delta q_2}{k_o} - \frac{(1 - s^2)}{s}$$

$$\phi_2 \sim -\frac{\pi}{2} + s \frac{\delta q_2}{k_o}$$

and

$$\theta = 2\pi - \frac{\delta q_2}{k_o s}$$

From this we deduce that

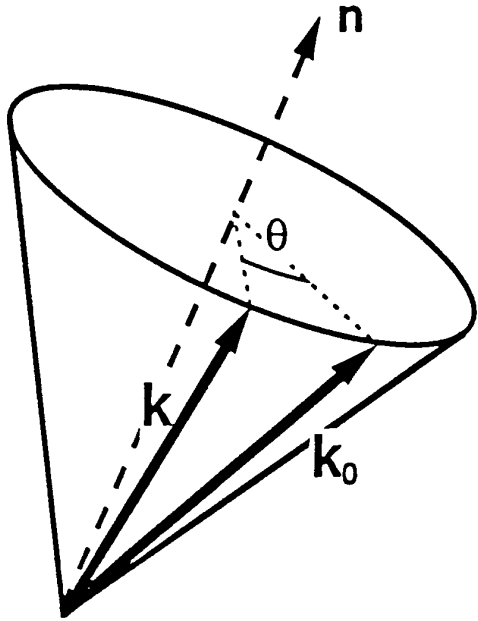
$$|\delta q_1| \sim \frac{\psi}{(1 - \psi^2)^{\frac{1}{2}}} \frac{\delta q_2^2}{2k_o} \quad (\text{C.16})$$

It is reassuring to note that this limiting form of the result is in agreement with that obtained in the previous appendix (eq B.19)

References

- 1) Walker, J. L. Range Doppler Imaging of Rotating Objects, IEEE AES-16, 1, 23 (1980).
- 2) Tough, R. J. A., The coordinate-free Representation of Rotational Motions, RSRE Memorandum 4445 (1991).
- 3) Jeffreys, H. and Jeffreys, B. S., Methods of Mathematical Physics. Chaps 2,3, University Press, Cambridge (1966).
- 4) Wehner, D. R., High Resolution Radar, Chap. 7, Artech House, Norwood MA, (1987).
- 5) Goldstein, H., Classical Mechanics, Addison Wesley, New York (1950).
- 6) Brink, D. M. and Satchler, G. R., Angular Momentum, Clarendon Press, Oxford (1968).
- 7) Wigner, E. P., Group Theory and its Application to the Quantum Mechanics of Atomic Spectra, Academic Press, New York (1959).

INTENTIONALLY BLANK



$$\underline{k} = M(\underline{n}, \theta) \cdot \underline{k}_0$$

Figure 1. The vector \underline{k}_0 is rotated about an axis \underline{n} into \underline{k} , lying on the surface of a cone.

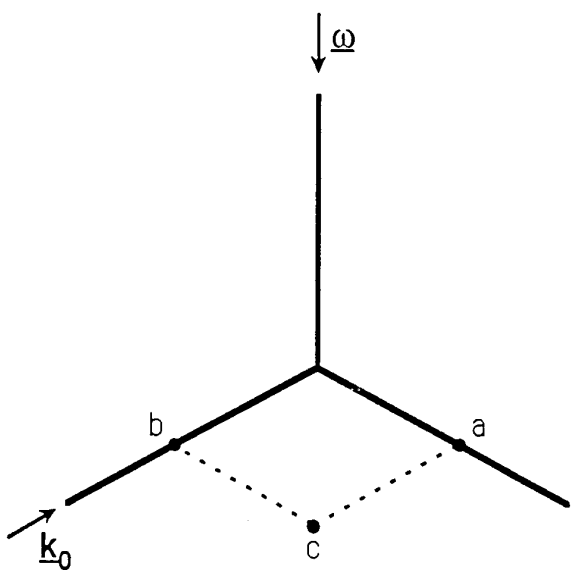


Figure 2(a)
Simulation Case 1
Radar and target geometry

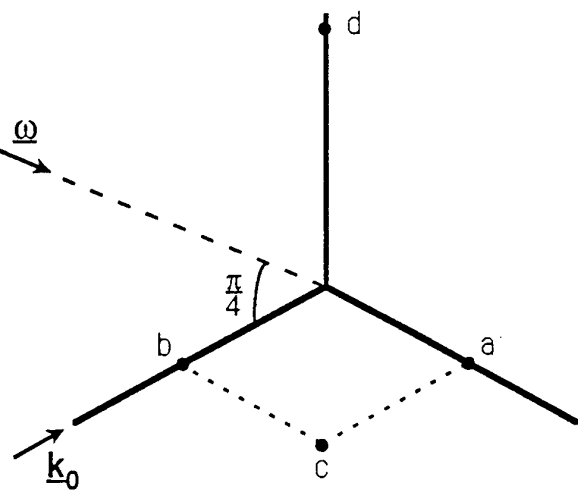


Figure 2(b)
Simulation Case 2
Radar and target geometry

Target coordinates:

$$a: (0, 67, 0), \quad b: (67, 0, 0)$$

$$c: (67, 57, 0)$$

Radar parameters:

Centre frequency $f_0 = 10$ GHz,

Target rotation rate = 4° s⁻¹,

Target coordinates:

$$a: (0, 67, 0), \quad b: (67, 0, 0)$$

$$c: (67, 67, 0), \quad d: (0, 0, 133)$$

Standard deviation of bandwidth:

$$\sigma_f = 75 \text{ MHz}$$

Standard deviation of integration time

$$\sigma_t = 125 \text{ mS.}$$

The radar transmission is of the wide instantaneous bandwidth type, rather than stepped frequency.

Case 1

| | (0,0,0) | | (0,67,0) | | (67,0,0) | | (67,67,0) | |
|-----------------------|---------|-------|----------|-------|----------|-------|-----------|--------|
| | act | pred | act | pred | act | pred | act | pred |
| $\langle x^2 \rangle$ | 0.10 | 0.101 | 0.42 | 0.442 | 0.10 | 0.101 | 0.42 | 0.442 |
| $\langle y^2 \rangle$ | 0.073 | 0.075 | 0.31 | 0.326 | 0.39 | 0.415 | 0.65 | 0.667 |
| $\langle xy \rangle$ | 0 | 0 | 0 | 0 | 0 | 0 | -0.33 | -0.342 |

Case 2

| | (0,0,0) | | (0,67,0) | | (67,0,0) | | (67,67,0) | | (0,0,133) | |
|-----------------------|---------|-------|----------|-------|----------|-------|-----------|--------|-----------|-------|
| | act | pred | act | pred | act | pred | act | pred | act | pred |
| $\langle x^2 \rangle$ | 0.10 | 0.101 | 0.26 | 0.272 | 0.10 | 0.101 | 0.267 | 0.272 | 0.10 | 0.101 |
| $\langle y^2 \rangle$ | 0.15 | 0.149 | 0.39 | 0.401 | 0.31 | 0.320 | 0.56 | 0.572 | 0.79 | 0.828 |
| $\langle xy \rangle$ | 0 | 0 | 0 | 0 | 0 | 0 | -0.162 | -0.171 | 0 | 0 |

Table 1

Comparison of the point spread function variance from simulation and theory.

(act = actual value from simulation;
pred = prediction from theory. Units m^2)

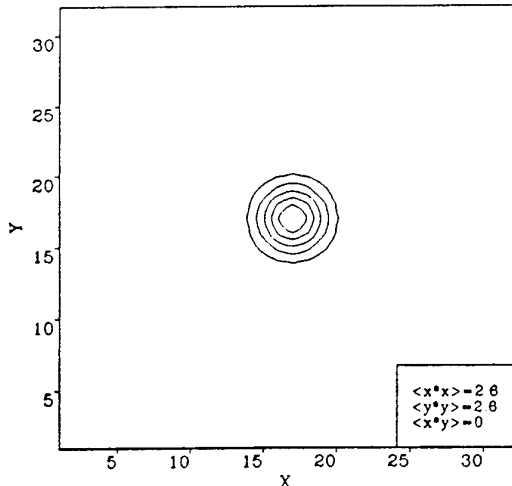
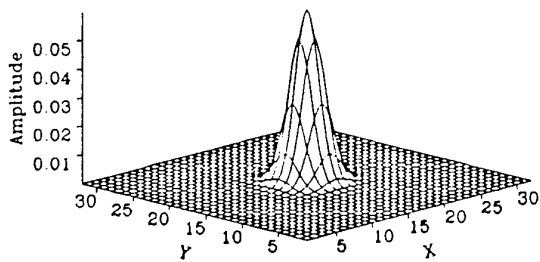
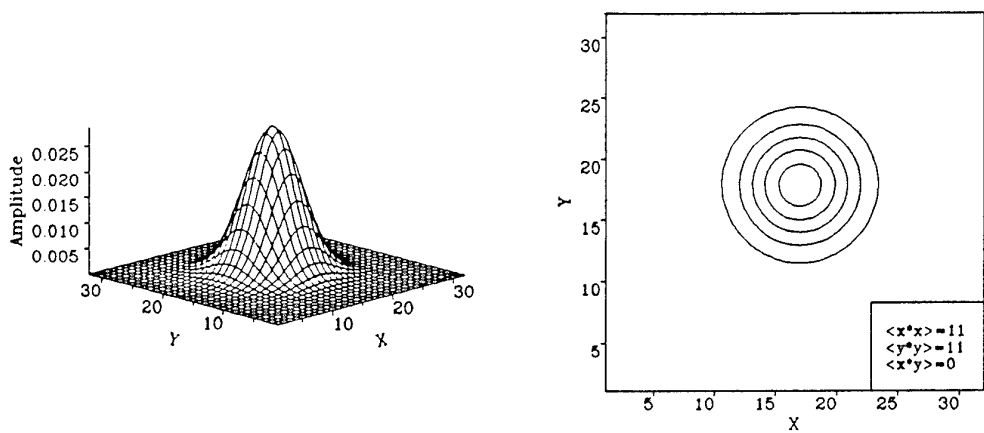
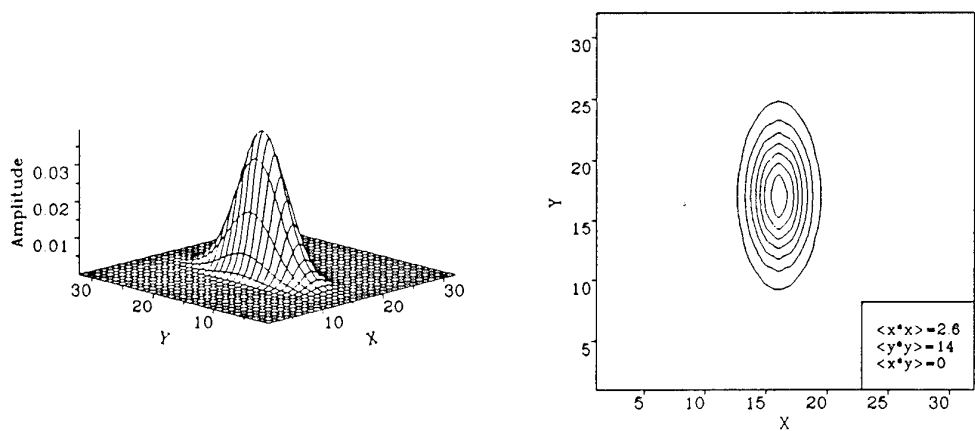


Figure 3: Point spread function of scatterer at the origin for case 1 (Figure 2(a))
Units for x axis: 0.195m. Units for y axis: 0.168m.

(a) SCATTERER AT (0,67,0)



(b) SCATTERER AT (67,0,0)



(c) SCATTERER AT (67,67,0)

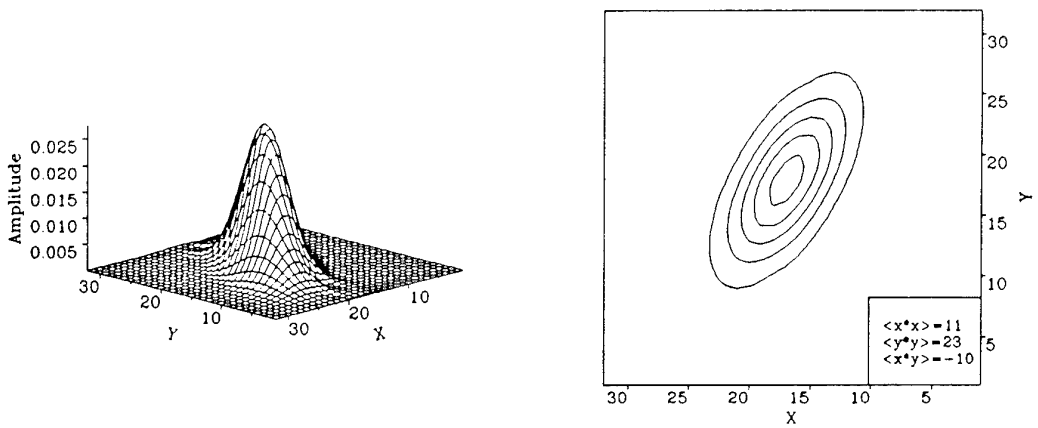
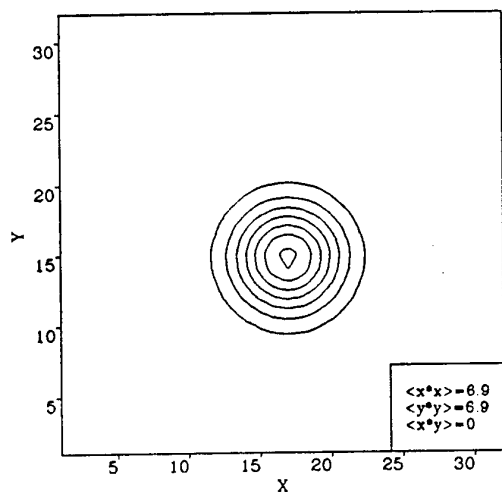
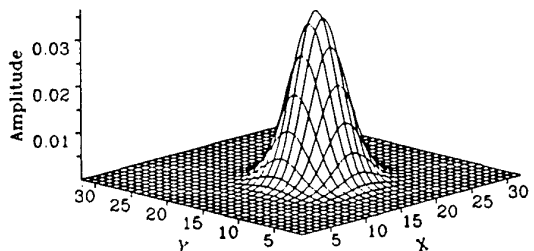


Figure 4: Point spread function of scatterers (a),(b), and (c) for case 1
Units for x axis = 0.195m. Units for y axis = 0.168m.

(a) SCATTERER AT (0,67,0)



(b) SCATTERER AT (67,0,0)

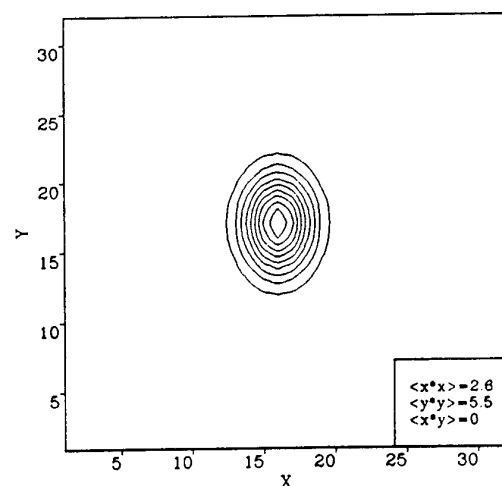
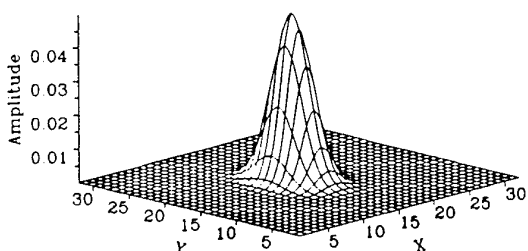
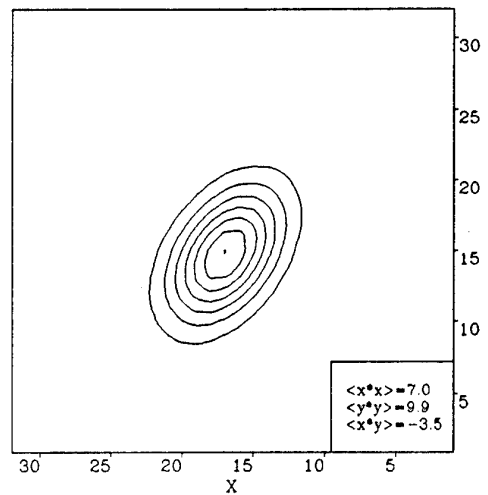
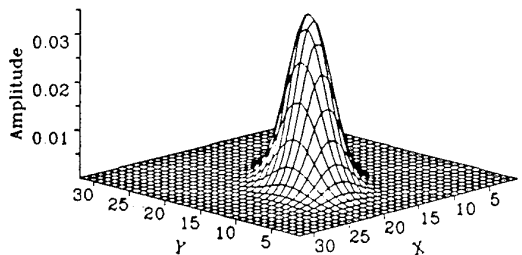


Figure 5: Point spread function of scatterers (a) and (b) for case 2
Units for x axis = 0.195m. Units for y axis = 0.237m.

(c) SCATTERER AT (67,67,0)



(d) SCATTERER AT (0,0,134)

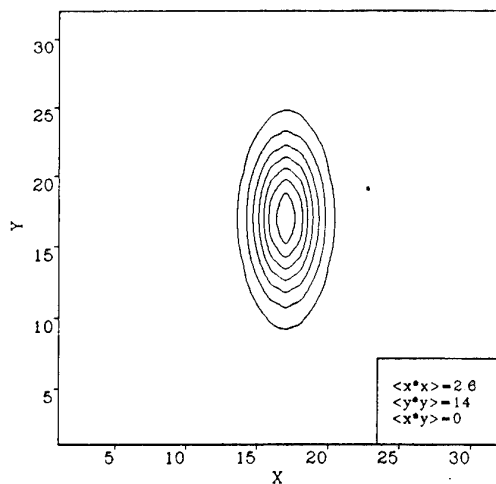
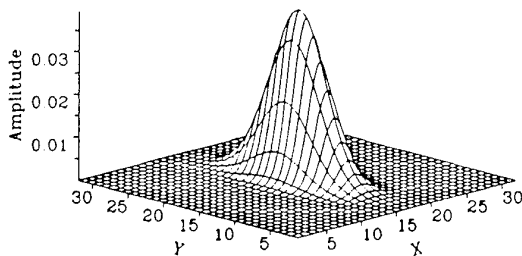


Figure 6: Point spread function of scatterers (c) and (d) for case 2
Units for x axis = 0.195m. Units for y axis = 0.237m.

References

- 1) Walker, J. L. Range Doppler Imaging of Rotating Objects, IEEE AES-16, 1, 23 (1980).
- 2 Tough, R. J. A., The coordinate-free Representation of Rotational Motions, RSRE Memorandum 4445 (1991).
- 3) Jeffreys, H. and Jeffreys, B. S., Methods of Mathematical Physics. Chaps 2,3, University Press, Cambridge (1966).
- 4) Wehner, D. R., High Resolution Radar, Chap. 7, Artech House, Norwood MA, (1987).
- 5) Goldstein, H., Classical Mechanics, Addison Wesley, New York (1950).
- 6) Brink, D. M. and Satchler, G. R., Angular Momentum, Clarendon Press, Oxford (1968).
- 7) Wigner, E. P., Group Theory and its Application to the Quantum Mechanics of Atomic Spectra, Academic Press, New York (1959).

INTENTIONALLY BLANK

REPORT DOCUMENTATION PAGE

DRIC Reference Number (if known)

Overall security classification of sheet **UNCLASSIFIED**
(As far as possible this sheet should contain only unclassified information. If it is necessary to enter classified information, the field concerned must be marked to indicate the classification, eg (R), (C) or (S).

| | | |
|--|---|---------------------|
| Originators Reference/Report No. MEMO 4532 | Month OCTOBER | Year 1991 |
| Originators Name and Location DRA, ST ANDREWS ROAD MALVERN, WORCS WR14 3PS | 1114 RSRE - MEMO - 4532 1111 | |
| Monitoring Agency Name and Location | | |
| Title A THEORY FOR HYBRID SAR/ISAR RADAR IMAGING 1118 | | |
| Report Security Classification UNCLASSIFIED | Title Classification (U, R, C or S) U | |
| Foreign Language Title (in the case of translations) | | |
| Conference Details | | |
| Agency Reference | Contract Number and Period | |
| Project Number | Other References | |
| Authors TOUGH, R J A; WARD, K D 29 | Pagination and Ref vp | |
| Abstract <p>A unified treatment of the SAR and ISAR imaging processes is presented, in which each emerges as a special case of a more general hybrid SAR/ISAR process. Several such special cases are considered, demonstrating the simplicity and flexibility of our analysis whose results are also verified directly by computer simulation.</p> | | |
| Abstract Classification (U, R, C or S) U | | |
| Descriptors | | |
| Distribution Statement (Enter any limitations on the distribution of the document) UNLIMITED | | S80/48 |

INTENTIONALLY BLANK